Wave-packet propagation in a graphene geometric diode

Wave-packet propagation in a graphene geometric diode

M. Andelkovic,[1] Kh. Yu. Rakhimov,[2,3,4,*] A. Chaves,[5] G. R. Berdiyorov,[6] and M. Milosevic[1]

[1] *Department of Physics, University of Antwerp, Groenenborgerlaan 171, 2020 Antwerpen, Belgium*
[2] *University of Geological Sciences, 64 Olimlar St., Tashkent 100125, Uzbekistan*
[3] *Arifov Institute of Ion-Plasma and Laser Technologies, 33 Durmon yuli St., Tashkent 100125, Uzbekistan*
[4] *Institute of Materials Science SPA "Physics-Sun", 2-B Chingiz Aitmatov St., Tashkent 100084, Uzbekistan*
[5] *Departamento de Física, Universidade Federal do Ceará, Caixa Postal 6030, Campus do Pici, 60455-900 Fortaleza, Ceará, Brazil*
[6] *Qatar Environment and Energy Research Institute, Hamad Bin Khalifa University, Doha, Qatar*

(Dated: November 21, 2022)

Dynamics of electron wave-packets is studied using the continuum Dirac model in a graphene geometric diode where the propagation of the wave packet is favored in certain direction due to the presence of geometric constraints. Clear rectification is obtained in the THz frequency range with the maximum rectification level of 3.25, which is in good agreement with recent experiments on graphene ballistic diodes. **The rectification levels are considerably higher for systems with narrower channels. In this case, the wave packet transmission probabilities and rectification rate also strongly depend on the energy of the incident wave packet, as a result of the quantum nature of energy levels along such channels.** These findings can be useful for fundamental understanding of the charge carrier dynamics in graphene geometry diodes.

I. INTRODUCTION

Geometric diodes [1] are based on the concept of rectifying the charge carriers in the ballistic regime due to the asymmetry imposed by the geometric constraints without the presence of any built-in potential [2]. Graphene [3–5] is considered to be the most promising materials for geometric diode development due to the following properties: i) exceptionally high charge carrier mobility, which makes this material suitable for high-frequency applications [6, 7]; ii) intrinsic long mean free path [8], which enables creating graphene-based ballistic rectifiers using conventional lithographic techniques [9]; iii) reduced capacitance due to the planar architecture, which increases the cut-off frequency of the device [10–12]; iv) low resistance [13] which contributes to rectification of small amplitude signals, thus reducing performance-limiting electrical noise in the system [14]. Graphene-based geometric diodes have already been demonstrated experimentally [6, 9, 11, 13, 15, 16]. Most of the graphene geometry diodes have been created by direct nanostructuring the material so that electrons are scattered only at the graphene edges [17]. However, recent computer simulations predict the possibility of creating high performance graphene geometry diodes through spatial chemical doping without physical constrictions [18].

There are several model approaches to describe geometric diodes, such as Landauer-Büttiker formalism, which is based on carrier transmission analysis [18, 19], and a Monte Carlo method which uses Drude-like transport of charge carriers [13, 20]. The former approach is mainly applied in purely ballistic case without accounting for momentum relaxation, whereas the latter formalism includes momentum relaxation in quasi-ballistic rectifiers. Here, we study the dynamics of electron wave packets in graphene geometric diode (see Fig. 1) using the relativistic Dirac equations of motion, which is an effective approach in describing the propagation of electron wave packets in graphene. [21] **We found clear rectification of the wave packet with rectification factor being larger for narrower channels. Also, for such narrow channels, the rectification rate can be controlled by the energy of the incident wave packet, which is experimentally related to the Fermi level and potential difference along the system. Maximum rectification level of 3.25 is obtained for narrow channels, while for thicker channels we find a rectification rate ≈2.4, which is in good agreement with recent experiments on graphene ballistic diodes [22].** The time response of the considered graphene geometric diode was found to be in THz range of the spectrum as was shown in previous

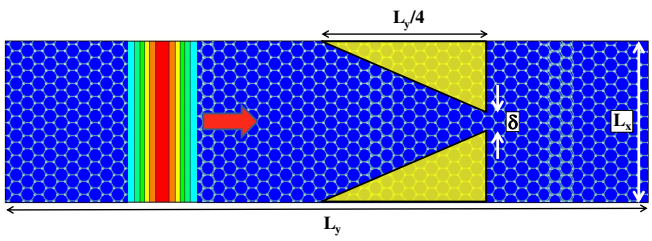

FIG. 1: Schematics of graphene geometric diode created by a geometric constraint (shaded areas), which favors the motion of the wave packet along the forward direction (indicated by an arrow).

*Electronic address: kh.rakhimov@gmail.com

experiments [6].

II. MODEL SYSTEM AND COMPUTATIONAL DETAILS

Figure 1 shows our model system consisting of a graphene monolayer with lateral dimensions L_x and L_y. An electron wave packet in the form of a Gaussian wave front is rectified due to the presence of the sloped arrowhead (shaded area in Fig. 1) with the constricted neck region of size δ. Figure 1 shows the schematic of our model diode system, where the geometric constraints are created by potential gating of the the graphene sheet to obtain different wave packet transmission probabilities. This inverse arrowhead constriction is crucial for the operation of the device as it determines the forward (i.e., easy transmitting) direction for the charge carriers (from left to right in Fig. 1). Efficiency of such a geometry has already been shown as compared to some of the other graphene-based ballistic geometric diodes [22].

The Gaussian wave packet, which has constant amplitude along the x-direction and width a_y along the y-direction, is represented as

$$\Psi(x,y,0) = N \begin{pmatrix} 1 \\ i \end{pmatrix} e^{iky - \frac{y^2}{2a_y^2}}, \tag{1}$$

where $(1 \quad i)^T$ is a pseudo-spinor, N is a normalization constant and k is the wave vector. In graphene, k is related to the energy of the wave packet E as $k = E/\hbar v_F$ with v_F being the Fermi velocity. The pseudo-spinor is chosen such that $\langle\sigma_y\rangle = 1$ and $\langle\sigma_x\rangle = \langle\sigma_z\rangle = 0$, which defines the wave packet propagation along the y-direction [23]. We do not consider circularly symmetric wave packets to avoid complex dynamics of the wave packet (e.g., the trembling motion – *zitterbewegung* [23, 24]) in the considered model system, which can make it difficult to estimate the rectification properties of the diode.

We apply the following time-evolution operator to propagate the initial Gaussian wave packet:

$$\Psi(x,y,t+\Delta t) = e^{-\frac{i}{\hbar}H\Delta t}\Psi(x,y,t), \tag{2}$$

where the time-independent Hamiltonian H describes the low energy electrons in graphene [25]

$$H = v_F\vec{\sigma}\cdot(\vec{p}) + V(x,y)\sigma_z. \tag{3}$$

In this equation, $\vec{\sigma}$ is the Pauli vector and the wave functions are represented by pseudo-spinors $\Psi = (\Psi_A, \Psi_B)^T$ with Ψ_A and Ψ_B being the probability of finding the electron in the A and B sub-lattices, respectively.

We use the split-operator technique [26, 27] to separate the energy terms in the time-evolution operator as

$$\exp\left[-\frac{i}{\hbar}H\Delta t\right] = \exp\left[-\frac{i}{2\hbar}V(x,y)\sigma_z\Delta t\right]\exp\left[-\frac{i}{\hbar}v_F\vec{p}\cdot\vec{\sigma}\Delta t\right]\exp\left[-\frac{i}{2\hbar}V(x,y)\sigma_z\Delta t\right], \tag{4}$$

and neglect the terms of order higher than $O(\Delta t^3)$. This approach has several advantages, such as the possibility of performing multiplications of real and reciprocal spaces independently and rewriting the exponentials of the Pauli matrices exactly [21, 28], which makes the calculations less demanding.

The diode constriction, with structural asymmetry in the shape of a triangle, is included in the model by introducing a high value effective mass-related potential term in the Dirac equation in the shaded regions of Fig. 1. This kind of potential exhibits different sign for pseudo-spin up and down components in the diagonal of the Dirac Hamiltonian for low energy electrons in graphene, which results in a gap opening [25] only in the shaded triangular regions of the diode, which scatters the incoming electron wave packets.

Periodic boundary conditions are used in both lateral directions and the wave packets are propagated with a time step of 0.1 fs. The probabilities are calculated before and after the constrictions area, where the latter one is considered as a transmission probability of the wave packet. The length of the sample along the wave packet propagation direction is always 4 times larger than the size of the scattering area to avoid the boundary effects on the calculated probabilities. **All simulations are performed assuming a wave packet width a_y = 20 nm [29].**

III. RESULTS AND DISCUSSIONS

We start by considering the propagation of the Gaussian wave front along the y-direction. **Figure 2 shows the probabilities of finding the electron before (blue curve) and after (red curve) the constriction as a function of time for the forward direction, assuming a wave packet energy E= 100 meV and neck size δ = 28 nm.** Once approaching the "barrier" area (panel 1 in Fig. 2), the dynamics of the wave packet is restricted to the funnel-like constriction region

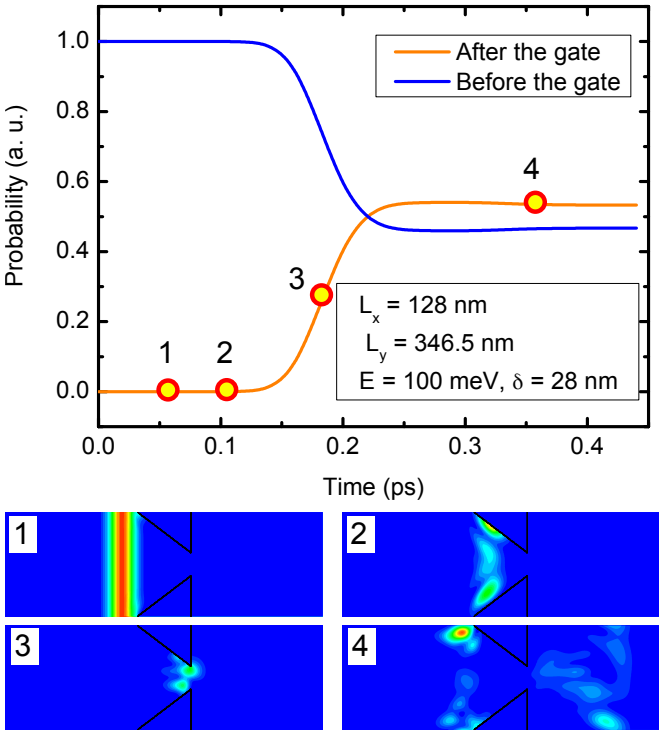

FIG. 2: Probabilities of finding the electron before (blue curve) and after (red curve) the constriction region as a function of time, when the wave packet propagates in forward direction. Sample parameters and wave function energy are given in the main panel. Panels 1-4 show the snapshots of the wave-packet propagation at times indicated in the main panel.

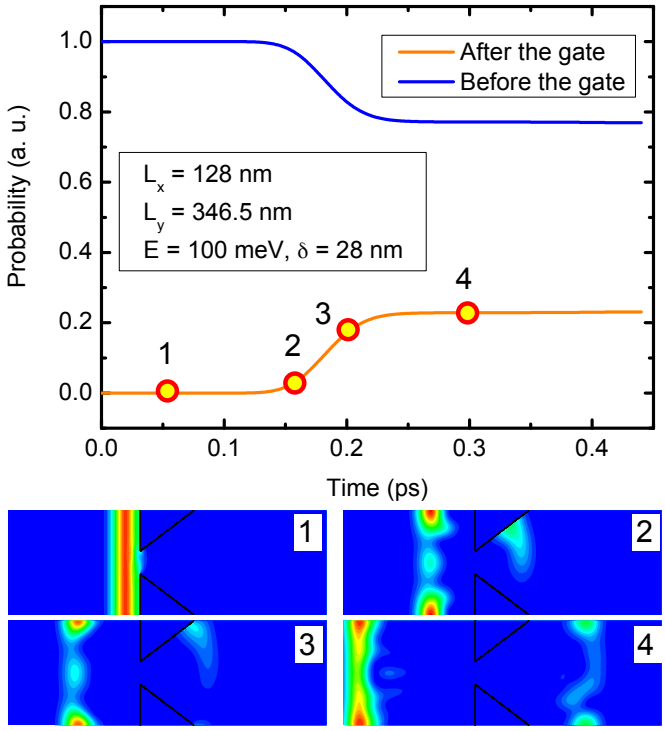

FIG. 3: The same as in Fig. 2, but for the reverse direction of the wave packet.

and exhibits specular reflections at the edges (panel 2). During this period the probability of the wave packet after the constriction area increases slightly. At 0.3 ps after the initial release, the wave packet reaches the neck of the geometric constriction (panel 3) and the probability increases sharply. **For the given geometrical parameters and the parameters of the wave packet, the probability of the transmitted wave packet (more than 50%) is larger than the one for the reflected wave packet (see panel 4).** See supplemental online video 1 for the complete dynamics of the wave packet.

Figure 3 shows the probabilities of the wave packet as a function of time to cross the sample along the reverse direction. Panels 1-4 are the snapshots of the wave packet at time intervals indicates in the main panel to show the wave packet evolution along this "hard" direction. As expected, the wave packet face larger resistance in the reverse direction as compared to the forward direction. Indeed, as seen from the top panel, the probability of the transmitted wave packet is much smaller than the probability of the reflected wave packet: less than 30% of the wave packet is transmitted through the "barrier" area (see panel 1-4 in Fig. 3). This is because of the reflection of the wave packet by the vertical blocks (see supplemental online video 2). Thus, the presence of the funnel-like construction gives different wave packet transmission probabilities in the forward and reverse directions with the rectification ratio higher than 2.

In Fig. 4(a), we plot the rectification level, i.e. the ratio between transmission probabilities through the system in the forward ("easy") and backward ("hard") directions, as a function of neck size δ of the triangular scattering center. The latter is crucial for the performance of graphene-based geometric diodes and can be considered as an important parameter for successful design of the devices. The rectification level is between 1.5 and 3, which is in good agreement with previous experimental findings for graphene-based ballistic diodes [22]. The maximum in the rectification (3.35) for all cases investigated here is reached at 7 nm for $E = 75$ meV. At a larger energy, $E = 150$ meV, the maximum rectification level is slightly lower, and is obtained for $\delta = 27$ nm. The system exhibits different (non-monotonic) dependence of the rectification level on the neck size for different energies. The mechanism for the obtained rectification is the higher transmission probability of wave packets in the forward direction due to the guided reflection off the diagonal walls than the transmission probabilities in the reverse direction, where the wave packets backscatters from the vertical walls.

Next we consider the case when the wave packet propagates with different incident energies. Fig-

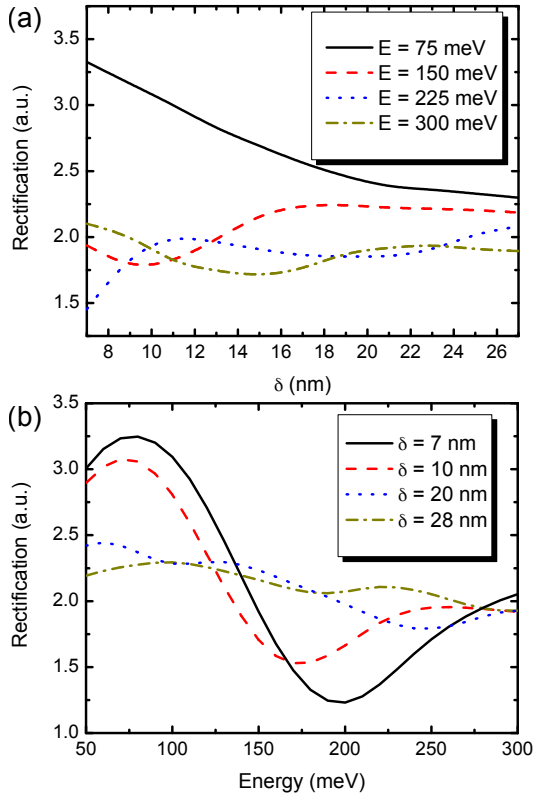

FIG. 4: Rectification ratio as a function (a) of the separation δ between the triangles, assuming different values of energy E of the propagating wave packet, and (b) of the energy E, assuming different values of the separation δ.

ure 4(b) shows the rectification level as a function of the incident wave front energy. The neck size is considered with different values δ, as labelled in the panel. For all energy values considered here, the wave packet still funnels along this forward direction through reflections at the sloped arrowhead boundaries. Reduced transmission is also obtained along the "hard" direction. By controlling the incident electron energy, which can be done via the Fermi level of the system, one can tune even better the rectification device. Results in Fig. 4(b) confirm that the 3.35 rectification for $E = 75$ meV in a 7 nm constriction is indeed the best case scenario for this device within the energy range and lengthscales considered here.

Just like in the case of rectification as a function of the constriction length δ in Fig. 4(a), the rectification in Fig. 4(b) also slightly oscillates as a function of the wave packet energy. However, the oscillations are demonstrated to be strongly damped as the neck size increases, so that the results for $\delta = 28$ nm exhibits only very weak oscillations, with shorter period. This helps us to understand the origin of these oscillations: in fact, they are reminiscent of the oscillations observed in quantum barriers for incident energies slightly above the barrier height. [30] In the lengthscale of few nanometers, quantum mechanics effects are important in the neck of the structure illustrated in Fig. 1. The region in between triangles may present a minimum energy for incident electrons, which thus work as an additional energy barrier for the incident wave packet, whose transmission probability would present maxima at resonant energies. Similar oscillations are observed e.g. in graphene-based quantum point contacts as well, see Refs. [31, 32]. Indeed, as δ increases, quantum confinement effects become less important, thus explaining the weak oscillations observed in Fig. 4(b) for $\delta = 20$ nm and 28 nm.

Notice that, regardless of the size of the neck region at the end of the arrowhead and the direction of the motion of the wave packets, the transmission time for the wave packet is around 0.3 ps. This indicates that the considered systems operate at THz frequencies, which can be further improved to reach the optical frequencies by changing the geometrical parameters of the samples.

IV. CONCLUSIONS

We use the continuum Dirac approach to study the propagation of Gaussian wave packets in a graphene geometric diode where the rectification is obtained due to the presence of an arrowhead geometric constraint to favor the motion of the wave packet in a certain direction. **Depending on the structural parameters of the sample, the maximum rectification level of 3.35 is obtained, which is in good agreement with previous experiments [9, 22]. For narrow constrictions between the triangular scattering regions forming the arrowhead, the rectification level of the device oscillates as a function of the wave packet energy, which is reminiscent of quantum resonances in potential barriers and quantum point contacts.** In any case, the devices operates at frequencies in the THz range of the spectrum. However, we point out the responsivity of the considered samples are low: the transmission probability of the wave packet along the forward direction is less than 100 % and there is always finite transmission probability in the other direction [33]. These findings can be useful in understanding the dynamics of the charge carriers in graphene geometric diodes and the fundamental limitations in the response time of the devices.

V. ACKNOWLEDGEMENTS

Computational resources were provided by the research computing center at University of Antwerp. A. C. acknowledges financial support from the Brazilian Council of Research (CNPq), through the PQ and UNIVERSAL programs, and from the Research Foundation-Flanders (FWO).

[1] G. Moddel, Geometric diode, applications and method, US Patent Application 20110017284, 2009.

[2] A. M. Song, A. Lorke, A. Kriele, J. P. Kotthaus, W. Wegscheider, M. Bichler, Nonlinear electron transport in an asymmetric microjunction: a ballistic rectifier, Phys. Rev. Lett. 80 (1998) 3831-3834.

[3] K. S. Novoselov, A. K. Geim, S. V. Morozov, D. Jiang, Y. Zhang, S. V. Dubonos, I. V. Grigorieva, and A. A. Firsov, Electric field effect in atomically thin carbon films, Science 306 (2004) 666.

[4] A. K. Geim and K. S. Novoselov, The rise of graphene, Nat. Mater. 6 (2007) 183.

[5] K. S. Novoselov, V. I. Fal'ko, L. Colombo, P. R. Gellert, M. G. Schwab, and K. Kim, A roadmap for graphene, Nature 490 (2012) 192.

[6] G. Auton, D. B. But, J. Zhang, E. Hill, D. Coquillat, C. Consejo, P. Nouvel, W. Knap, L. Varani, F. Teppe, J. Torres, and A. Song, Terahertz Detection and Imaging Using Graphene Ballistic Rectifiers, Nano Lett. 17 (2017) 7015-7020.

[7] D. A. Bandurin, D. Svintsov, I. Gayduchenko, S. G. Xu, A. Principi, M. Moskotin, I. Tretyakov, D. Yagodkin, S. Zhukov, T. Taniguchi, K. Watanabe, I. V. Grigorieva, M. Polini, G. N. Goltsman, A. K. Geim, and G. Fedorov. Resonant terahertz detection using graphene plasmons. Nature Communications 9 (2019) 5392.

[8] A. H. Castro Neto, F. Guinea, N. M. R. Peres, K. S. Novoselov, and A. K. Geim, The electronic properties of graphene, Rev. Mod. Phys. 81 (2009)109.

[9] H. Wang, G. Jayaswal, G. Deokar, J. Stearns, P. M. F. J. Costa, G. Moddel, A. Shamim, CVD-Grown Monolayer Graphene-Based Geometric Diode for THz Rectennas. Nanomaterials 11 (2021) 1986.

[10] A. K. Singh, G. Auton, E. Hill, A. Song, Estimation of intrinsic and extrinsic capacitances of graphene self-switching diode using conformal mapping technique, 2D Mater. 5 (2018) 035023.

[11] Z. Zhu, S. Grover, K. Krueger, and G. Moddel, Optical rectenna solar cells using grapheme geometric diodes. PVSC 37 (2011) 2120-2122.

[12] S. Joshi, Z. Zhu , S. Grover, and G. Moddel, Infrared optical response of geometric diode rectenna solar cells. PVSC 38 (2012) 2976-2978.

[13] Z. Zhu, S. Joshi, S. Grover, and G. Moddel, Graphene geometric diodes for terahertz rectennas. J. Phys. D: Appl. Phys. 46 (2013) 185101.

[14] G. Auton, J. Zhang, R. K. Kumar, H. Wang, X. Zhang, Q. Wang, E. Hill and A. Song, Graphene ballistic nanorectifier with very high responsivity, Nature Communications 7 (2016) 11670.

[15] L. Vicarelli, M. S. Vitiello, D. Coquillat, A. Lombardo, A. C. Ferrari, W. Knap, M. Polini, V. Pellegrini, and A. Tredicucci, Graphene field-effect transistors as room-temperature terahertz detectors, Nat. Mater. 11 (2012) 865-871.

[16] A. K. Singh, G. Auton, E. Hill, and A. Song, Graphene based ballistic rectifiers, Carbon 84 (2015) 124-129.

[17] A. S. Mayorov, R. V. Gorbachev, S. V. Morozov, L. Britnell, R. Jalil, L. A. Ponomarenko, P. Blake, K. S. Novoselov, K. Watanabe, T. Taniguchi, and A. K. Geim, Micrometer-scale ballistic transport in encapsulated graphene at room temperature, Nano Lett. 11 (2011) 2396-2399.

[18] G. R.Berdiyorov and H. Hamoudi, Creating graphene geometry diodes through fluorination: First-principles studies, Comput. Mater. Sci. 188 (2021) 110209.

[19] J. Brownless, J. Zhang, A. Song, Graphene ballistic rectifiers: Theory and geometry dependence. Carbon 168 (2020) 201-208.

[20] J. Stearns and G. Moddel, Simulation of Z-Shaped Graphene Geometric Diodes Using Particle-in-Cell Monte Carlo Method in the Quasi-Ballistic Regime, Nanomaterials 11 (2021) 2361.

[21] A. Chaves, G. A. Farias, F. M. Peeters, and R. Ferreira, The Split-Operator Technique for the Study of Spinorial Wavepacket Dynamics, Communications in Computational Physics 17 (2015) 850-866.

[22] V. H. Nguyen, D. C. Nguyen, S. Kumar, M. Kim, D. Kang, Y. Lee, N. Nasir, M. A. Rehman, T. P. A. Bach, J. Jung, and Y. Seo, Optimum design for the ballistic diode based on graphene field-effect transistors, npj 2D Materials and Applications 5 (2021) 89.

[23] A. Chaves, L. Covaci, Kh. Yu. Rakhimov, G. A. Farias, and F. M. Peeters, Wave-packet dynamics and valley filter in strained graphene, Phys. Rev. B 82 (2010) 205430.

[24] T. M. Rusin and W. Zawadzki, Zitterbewegung of relativistic electrons in a magnetic field and its simulation by trapped ions, Phys. Rev. D 82 (2010) 125031.

[25] A. H. Castro Neto, F. Guinea, N. M. R. Peres, K. S. Novoselov, and A. K. Geim, The electronic properties of graphene, Rev. Mod. Phys. 81 (2009) 109.

[26] M. H. Degani and J. P. Leburton, Single-electron states and conductance in lateral-surface superlattices, Phys. Rev. B 44 (1991) 10901.

[27] M. Suzuki, Fractal decomposition of exponential operators with applications to many-body theories and Monte Carlo simulations, Phys. Lett. A 146 (190) 319-323.

[28] Kh. Yu. Rakhimov, A. Chaves, G. A. Farias, and F. M. Peeters, Wavepacket scattering of Dirac and Schrödinger particles on potential and magnetic barriers, J. Phys.: Condens. Matter 23 (2011) 275801.

[29] T. Kramer, C. Kreisbeck, and V. Krueckl, Wave packet approach to transport in mesoscopic systems, Physica Scripta 82 (2010) 038101.

[30] E. Merzbacher, *Quantum Mechanics* (Wiley, New York, 1986).

[31] H. Overweg, H. Eggimann, X. Chen, S. Slizovskiy, M. Eich, R. Pisoni, Y. Lee, P. Rickhaus, K. Watanabe, T. Taniguchi, V. Fal'ko, T. Ihn, and K. Ensslin, Electrostatically Induced Quantum Point Contacts in Bilayer Graphene, Nano Lett. 18 (2018) 553.

[32] D. R. da Costa, A. Chaves, S. H. R. Sena, G. A. Farias, and F. M. Peeters, Valley filtering using electrostatic potentials in bilayer graphene, Phys. Rev. B 92 (2015) 045417.

[33] G. Moddel, Z. Zhu, S. Grover, S. Joshi, Ultrahigh speed graphene diode with reversible polarity, Solid State Commun. 152 (2012) 1842-1845.